A diurnal carbon engine explains ^{13}C-enriched carbonates without increasing the global production of oxygen

Emily C. Geyman[a,1] and Adam C. Maloof[a]

[a]Department of Geosciences, Princeton University, Princeton, NJ 08544

Edited by Donald E. Canfield, Institute of Biology and Nordic Center for Earth Evolution, University of Southern Denmark, Odense M., Denmark, and approved October 8, 2019 (received for review May 21, 2019)

In the past 3 billion years, significant volumes of carbonate with high carbon-isotopic ($\delta^{13}C$) values accumulated on shallow continental shelves. These deposits frequently are interpreted as records of elevated global organic carbon burial. However, through the stoichiometry of primary production, organic carbon burial releases a proportional amount of O_2, predicting unrealistic rises in atmospheric pO_2 during the 1 to 100 million year-long positive $\delta^{13}C$ excursions that punctuate the geological record. This carbon–oxygen paradox assumes that the $\delta^{13}C$ of shallow water carbonates reflects the $\delta^{13}C$ of global seawater-dissolved inorganic carbon (DIC). However, the $\delta^{13}C$ of modern shallow-water carbonate sediment is higher than expected for calcite or aragonite precipitating from seawater. We explain elevated $\delta^{13}C$ in shallow carbonates with a diurnal carbon cycle engine, where daily transfer of carbon between organic and inorganic reservoirs forces coupled changes in carbonate saturation (Ω_A) and $\delta^{13}C$ of DIC. This engine maintains a carbon-cycle hysteresis that is most amplified in shallow, sluggishly mixed waters with high rates of photosynthesis, and provides a simple mechanism for the observed $\delta^{13}C$-decoupling between global seawater DIC and shallow carbonate, without burying organic matter or generating O_2.

carbonates | carbon isotopes | chemostratigraphy | paleoclimate

Andros Island (Great Bahama Bank [GBB]), San Salvador (Bahamas), and Shark Bay (Western Australia) represent a wide range of seawater residence times and salinities, but all produce carbonate sediment $\sim 5‰$ higher than the $\delta^{13}C$ values of open marine waters (Fig. 1). Carbon-isotope enrichment factors for bicarbonate to inorganic calcite ($\sim 1.1‰$) and aragonite ($\sim 2.7‰$) are relatively insensitive to temperature and precipitation rate (1, 2) and only explain half of the elevated $\delta^{13}C$ signal observed in these shallow carbonate sediments. The most common explanation for the production of high $\delta^{13}C$ carbonate on a global (3) or local (4) scale involves increasing the export/burial of organic carbon relative to carbonate in order to leave the residual waters (from which carbonates are precipitated) enriched in ^{13}C. However, carbonate sediments on the GBB have low total organic carbon (TOC) ($\sim 0.3\%$) (5). Thus, the canonical organic burial explanation would require wholesale export of organic carbon off the shelf without depleting nutrients. However, carbonates produced on the GBB and exported to the periplatformal slope (6) also have low TOC (5), refuting the idea of significant organic-carbon export. We propose an alternative mechanism whereby photosynthesis still drives high $\delta^{13}C$ in shallow carbonates, even if all of the organic matter produced each day is respired at night, such that net organic-matter burial and nutrient depletion is zero.

On shallow banks, the 3 most important mechanisms for exchanging carbon into and out of the DIC pool are 1) carbonate precipitation/dissolution, 2) atmospheric gas exchange, and 3) photosynthesis/respiration. The relative contributions of these processes can be constrained by visualizing the carbon evolution of banktop seawater in a Deffeyes diagram (9) (Fig. 2*B*), since each mechanism induces a characteristic change in DIC and total alkalinity (TA) (Table 1). Observations of TOC (5) and DIC vs. TA (7) from the GBB constrain the relative sizes of the net carbonate, gas-exchange, and organic fluxes to be 62, 37, and $<1\%$, respectively (Fig. 2). Although the net burial of organic matter is close to zero, the flux of carbon between organic matter and the DIC pool over the course of a single diurnal (24-h) cycle can exceed the gross atmospheric and carbonate fluxes by over a factor of 20 in shallow carbonate environments (12–15). In other words, photosynthesis drives substantial perturbations to the carbonate system during the day, but respiration covers up the tracks each night.

The diurnal cycle of photosynthesis and respiration permits a $\delta^{13}C$ hysteresis (Fig. 3). As the sun rises, photosynthesis consumes CO_2 from the water column, driving up Ω_A. The maximum rate of carbonate precipitation (a function of Ω_A) is achieved as peak photosynthesis increases the $\delta^{13}C$ of residual DIC, leading to carbonate sediment enriched in ^{13}C. As night falls, aerobic respiration lowers the $\delta^{13}C$ of DIC but also depresses Ω_A, preventing significant carbonate production recording the low $\delta^{13}C$ values. The net effect of this diurnal carbon cycle hysteresis is to produce a shallow carbonate sediment record that has $\delta^{13}C$ higher than predicted for aragonite in equilibrium with average local seawater DIC.

Significance

We present stable carbon isotope ($\delta^{13}C$) data from modern carbonate sediment that require a decoupling of the carbon cycles in the global ocean versus shallow carbonate shelves. This realization is important because, for the first 97% of Earth history, many inferences about global paleoclimate and seawater chemistry rely on interpretations of shallow carbonates. We use modern observations and a simple model to show how ordinary diurnal carbon cycling in shallow waters is sufficient to produce anomalously positive $\delta^{13}C$ on shelves today, and in the geological record. Our results alleviate the need to interpret positive $\delta^{13}C$ excursions in the geological record as global reorganizations of the carbon cycle and instead link $\delta^{13}C$ to local and/or global paleoenvironmental and paleoecological controls.

Author contributions: E.C.G. and A.C.M. designed research, performed research, analyzed data, and wrote the paper.

The authors declare no competing interest.

This article is a PNAS Direct Submission.

Published under the PNAS license.

[1]To whom correspondence may be addressed. Email: egeyman@alumni.princeton.edu.

This article contains supporting information online at https://www.pnas.org/lookup/suppl/doi:10.1073/pnas.1908783116/-/DCSupplemental.

First published November 8, 2019.

Downloaded by guest on July 13, 2020

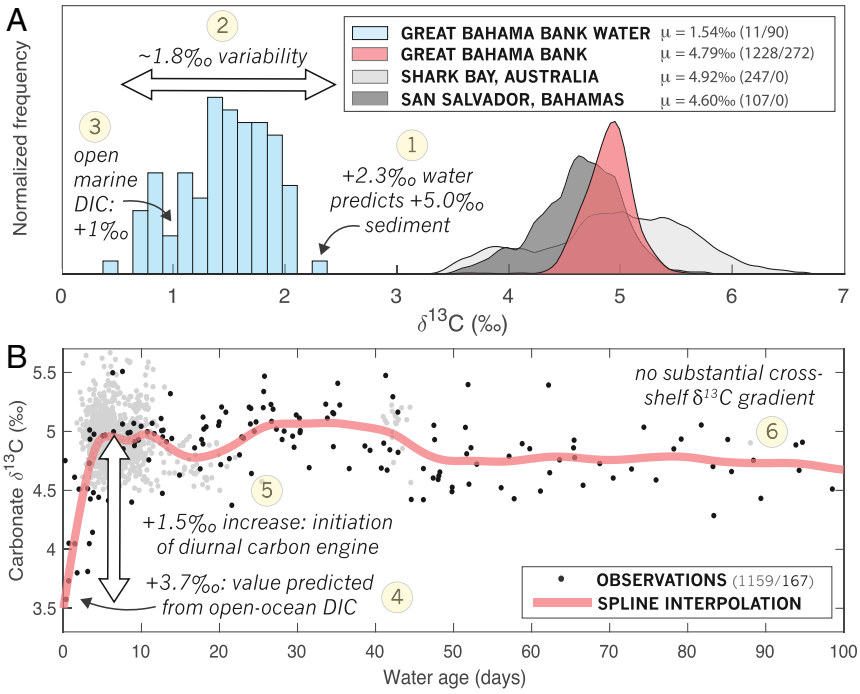

Fig. 1. Evidence in support of a diurnal organic carbon engine driving elevated $\delta^{13}C$ in shallow carbonates. (*A*) Three modern carbonate shelves produce bulk sediment with $\delta^{13}C$ that is too high to have precipitated directly from open marine waters. (*B*) The $\delta^{13}C$ values of GBB sediments rise abruptly near the shelf edge and remain high (>4.5‰) in the bank interior. The number of samples is denoted as this study/ref. 4 (1,159/167), and the banktop water ages in *B* are computed from a spatial interpolation of the ^{14}C ages in ref. 7 (Fig. 2). The diurnal organic carbon engine hypothesis predicts a number of observations consistent with the dataset: ① peak $\delta^{13}C$ of DIC should be high enough to precipitate aragonite with the dominant value of $\delta^{13}C \sim 5‰$; ② 1.8‰ variability in DIC is the same range predicted during one diurnal photosynthesis–respiration cycle (Fig. 3); ③ banktop waters have a $\delta^{13}C$ of DIC composition roughly equal to or higher than that of offshore waters; ④ sediments at the shelf edge have low $\delta^{13}C$, consistent with open marine DIC; ⑤ the rapid rise in sediment $\delta^{13}C$ near the platform edge captures the transition from the weak photosynthetic forcing (κ_p) characteristic of the open ocean to the strong photosynthetic forcing observed in shallow waters (Fig. 4); and ⑥ the lack of a significant cross-shelf $\delta^{13}C$ gradient reflects the balancing isotopic effects of carbonate precipitation (depletes residual DIC) and CO_2 gas escape (enriches residual DIC) (Fig. 7).

Carbon Model

To quantify the extent to which the temporal coupling between photosynthesis and carbonate precipitation increases the $\delta^{13}C$ of carbonate, we develop a simple mass balance model of the diurnal carbon engine (Fig. 3). To emphasize how the diurnal engine mechanism is distinct from the canonical treatment whereby net primary production drives elevated $\delta^{13}C$ in carbonates (3, 4), our diurnal engine returns 100% of the carbon sequestered in organic matter during the day back to the seawater each night (Fig. 3). The only prescribed forcing in the engine model is the daily photosynthetic transfer of carbon between the inorganic and organic reservoirs (κ_p). The gas exchange and carbonate fluxes are computed independently based on values of pCO_2 and Ω_A obtained in each time step using the carbonate-system calculation software

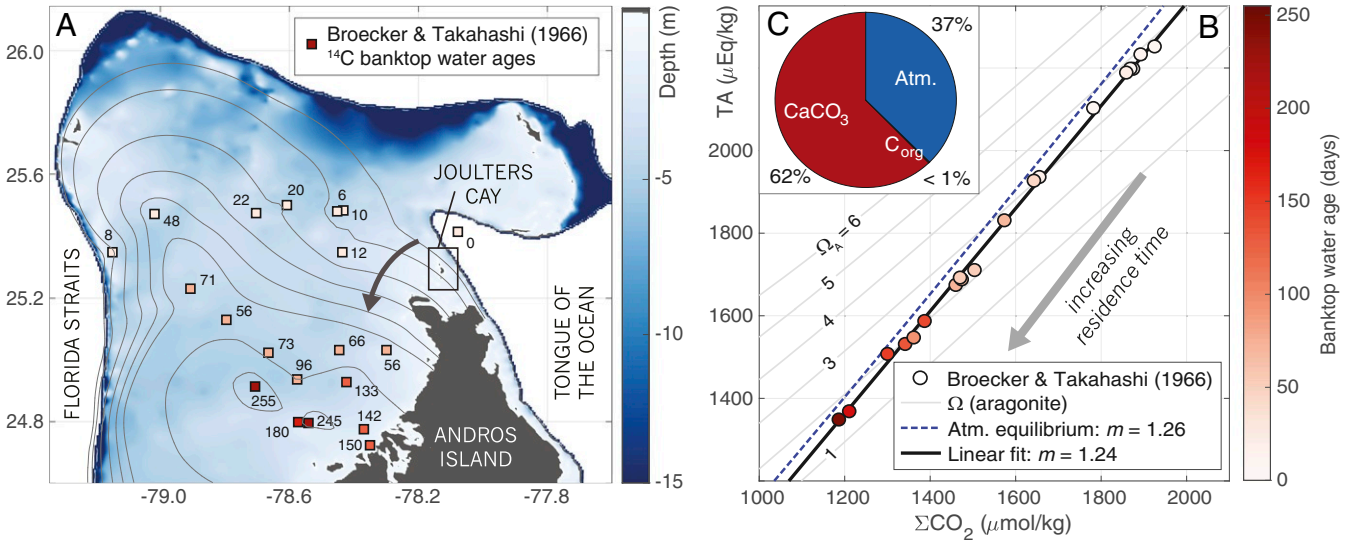

Fig. 2. Measurements of ^{14}C, ΣCO_2, and TA in seawater from the GBB (7) help to constrain the carbon fluxes in our model (Fig. 3). (*A*) Shallow waters and sluggish mixing on the GBB afford banktop residence times >250 days. Bathymetry from ref. 8. (*B*) ΣCO_2 and TA measurements produce a slope of m = 1.24 in the Deffeyes diagram (9) (Fig. 3*C*). The line representing atmospheric equilibrium was derived by allowing TA to vary from 1,200 to 2,375 μEq/kg (the *y*-axis range) and then using CO2SYS (10) to calculate ΣCO_2 if [CO_2 (aq)] = 317 ppm (i.e., equal to atmospheric pCO_2 at the time of the TA and ΣCO_2 measurements) (11). (*C*) We use the data in *B* and the observation that the mean TOC (weight %) of modern GBB sediment is 0.32±0.3% (1σ) (5) to constrain the sizes of the net carbonate precipitation, gas-escape, and C_{org} fluxes to be 62, 37, and <1%, respectively. We are able to compute the relative magnitudes of these 3 fluxes (2 unknowns, since $F_{carb} + F_{org} + F_{gas} = 1$) because: 1) TOC measurements (5) link organic carbon and carbonate burial: $F_{org} = 0.0107F_{carb}$; and 2) the slope in *B* reflects the relative contributions of carbonate precipitation, photosynthesis, and gas exchange, as each process induces a characteristic $\Delta TA{:}\Delta\Sigma CO_2$ ratio (Fig. 3*C* and Table 1).

Downloaded by guest on July 13, 2020

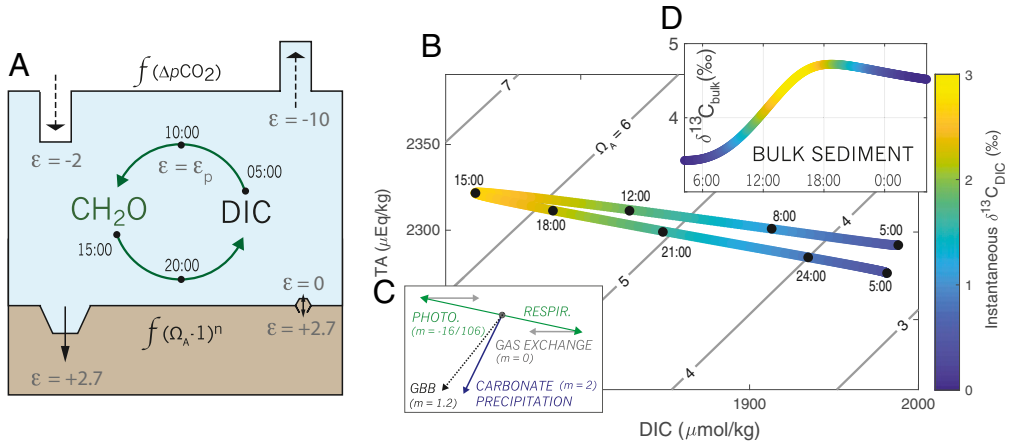

Fig. 3. The diurnal organic carbon engine. (*A*) A numerical mass balance model tracks the $\delta^{13}C$ composition and mass fluxes of carbon transferred through air–sea gas exchange, carbonate precipitation/dissolution, and photosynthesis/respiration. (*B*) Changes in TA and DIC for one 24-h engine model simulation. The changes in water chemistry induced by photosynthesis modulate the rates of carbonate production (a function of Ω_A) and air–sea gas exchange (a function of the pCO_2 gradient between the atmosphere and seawater). We use 5 common parameterizations for CO_2 gas exchange (17–21) and show that model results are insensitive to the chosen parameterization (*SI Appendix*, Fig. S14). Note that it is the slow rate of air–sea gas exchange that makes the diurnal organic carbon engine possible; the fact that CO_2 does not equilibrate with the atmosphere on 24-h cycles allows photosynthesis to drive up Ω_A. (*C*) The Deffeyes (9) diagram depicts the photosynthesis–respiration (slope = −16/106), carbonate precipitation–dissolution (slope = 2/1), and atmospheric equilibration (slope = 0) levers on TA and DIC (Table 1). Average seawater on the GBB (7) follows a slope of 1.24 (Fig. 2*B*). (*D*) The cumulative $\delta^{13}C$ composition of bulk sediment produced during the 24-h model simulation. Water with a starting composition of $\delta^{13}C_{DIC} = +1‰$ produces aragonite with an average $\delta^{13}C$ of +4.51‰. Note that the diurnal organic carbon engine still elevates $\delta^{13}C$ even if organic matter is more carbon-rich than a typical Redfield ratio. For example, if we model the end-member scenario in which banktop organic matter contains no N or P (see Fig. 4 legend), and thus photosynthesis no longer induces its modest increase in TA (Table 1), the engine model predicts that water with a starting composition of $\delta^{13}C_{DIC} = +1‰$ would produce aragonite with bulk $\delta^{13}C$ of +4.48‰. The reason for the relative insensitivity of the $\delta^{13}C$ enrichment to the nutrient-composition of organic matter is that the photosynthesis lever primarily increases Ω by drawing down ΣCO_2, not by adding TA (C). Notice in *D* that at night, when aerobic respiration returns 100% of the organic carbon back to the DIC pool, the instantaneous $\delta^{13}C_{DIC}$ falls to 0‰. However, since the low saturation state at night limits carbonate precipitation rates, the integrated, bulk sediment $\delta^{13}C$ decreases by $< 0.3‰$. The precipitated sediment preferentially records the highest $\delta^{13}C$ of DIC achieved during the diurnal cycle, rather than the mean $\delta^{13}C$ of DIC.

(CO2SYS) (10). To constrain the value of κ_p, we compile high-resolution time series of diurnal carbonate system variability from 21 shallow shelf locations around the world (Fig. 4).

In Fig. 3, we model carbonate precipitation as abiotic in the sense that we do not include the regulation of internal carbonate systems in calcifying organisms, which give rise to vital

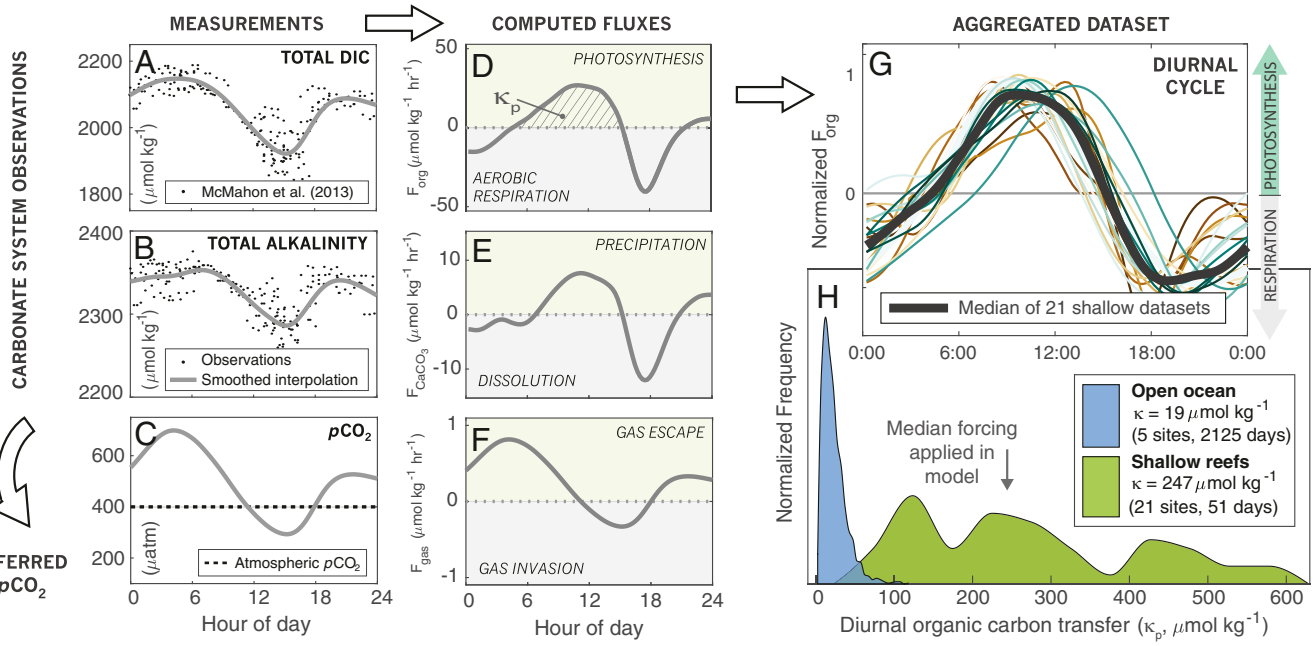

Fig. 4. An illustration of quantifying the diurnal organic carbon transfer (κ_p) from high-resolution observations of the carbonate system in modern environments. (*A* and *B*) Measurements of diurnal DIC and TA variability at Heron Island Lagoon (Great Barrier Reef) (15) as one example of the 21 shallow

Legend continued on following page

Downloaded by guest on July 13, 2020

environments collected in our database. (*C*) We use CO2SYS (10) to estimate pCO_2 from the TA and DIC data. (*D–F*) We compute the carbon fluxes due to photosynthesis/respiration (*D*), carbonate precipitation/dissolution (*E*), and gas exchange (*F*) from the TA, DIC, and pCO_2 observations (*SI Appendix*, Fig. S3). The calculated photosynthetic carbon flux (*D*) becomes the forcing of the engine model (Fig. 3). (*G*) A compilation of the 21 diurnal photosynthesis/respiration time series, normalized to the same amplitude to facilitate comparison of the timing of photosynthesis vs. respiration. (*H*) The diurnal organic-carbon transfer (κ_p), which represents the mass of carbon (per kilogram of seawater) that is sequestered in organic matter in the afternoon before aerobic respiration outpaces photosynthesis, computed for all 21 shallow reef and 5 open ocean settings in our dataset (*SI Appendix*, Table S3). Notice that κ_p typically is >10× larger in shallow reef environments than in open-ocean settings (22). We recognize that upwelling seawater often has insufficient phosphate to drive such large values of κ_p. For example, the average $[PO_4]$ of water 200- to 600-m-deep upwelling onto the GBB is ∼0.75 μmol/kg (*SI Appendix*, Fig. S7), which would support a κ_p of just 80 μmol/kg assuming the standard Redfield C:P = 106:1 (16). The large observed κ_p values likely reflect a combination of 1) active nutrient trapping on the shallow shelves (23–25) and 2) high carbon-to-nutrient ratios in banktop organic matter due to the abundance of microbial mats and their production of carbohydrate-rich extracellular polymeric substances (26–28). We take a simple empirical approach and drive our engine model with the median κ_p forcing observed in shallow environments (*H*).

effects (29). However, our mechanism is still important for biologically mediated precipitation because it explains how the $\delta^{13}C$ composition of banktop DIC—the starting material for biogenic carbonate—changes over the day. In other words, an active diurnal carbon cycle could elevate $\delta^{13}C$ in both abiotic and biotic carbonate.

Model Validation

The engine model (Fig. 3), forced by the median κ_p from carbonate reef environments (Fig. 4), along with the median values of water depth (30) and wind speed (8) on the GBB, successfully reproduces measured rates of carbonate production and air–sea gas exchange (7) (Fig. 5). In addition, the model produces carbonate with the same bulk $\delta^{13}C$ values we have measured in GBB sediment (Fig. 1*A*). The model also successfully explains the rapid rise in $\delta^{13}C$ at the platform edge (Fig. 1*B*), where waters transition from the weak photosynthetic forcing (low κ_p) characteristic of the open ocean to the strong forcing (high κ_p) observed in shallow waters (Fig. 4*H*). Finally, the large diurnal range in $\delta^{13}C$ of DIC observed in coral reef environments can be predicted accurately with the engine model forced by changes in TA and DIC measured in the same waters (Fig. 6*B*).

Drivers of Banktop $\delta^{13}C$ Variability

The extent to which $\delta^{13}C$ is elevated in carbonate sediment compared to mean seawater DIC is dominated by two factors: 1)

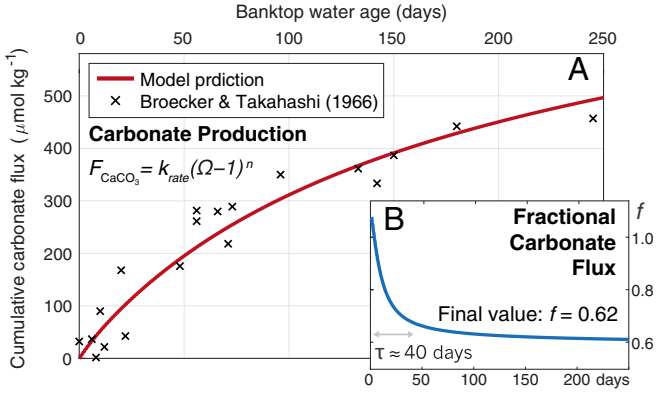

Fig. 5. A comparison between predictions from the carbon engine model (Fig. 3) and observational data from ref. 7 (Fig. 2). (*A*) The diurnal carbon engine model, run through 250 days of simulation, effectively describes rates of carbonate precipitation as a function of the days water has spent on the bank. Carbonate precipitation is parameterized as $F_{CaCO_3} = k_{rate}(\Omega - 1)^n$ (29, 31, 32), where $n \approx 1.7$ (31) and k_{rate}, which is poorly constrained for natural environments, is empirically optimized to fit the data from ref. 7 and is 9.0×10^{-9} mol m^{-2} s^{-1}. (*B*) Fractional carbonate flux $\left(f = \frac{F_{CaCO_3}}{F_{CaCO_3}+F_{gas}+F_{org}}\right)$ vs. banktop water age. The asymptotic fall of the curve in *B* reflects the slow rate of air–sea CO_2 gas exchange and equilibration. Note that only k_{rate}, one of many parameters in the model (*SI Appendix*, Tables S1 and S2), is tuned to data from ref. 7. Then, when the model is forced with independent observation-based estimates of κ_p and ϵ_p, and allowed to undergo air–sea gas exchange as a function of pCO_2, the model predicts $f = 0.62$, which is identical to the estimate derived from the data in ref. 7 (Fig. 2*C*) and serves as a test of self-consistency in our model system.

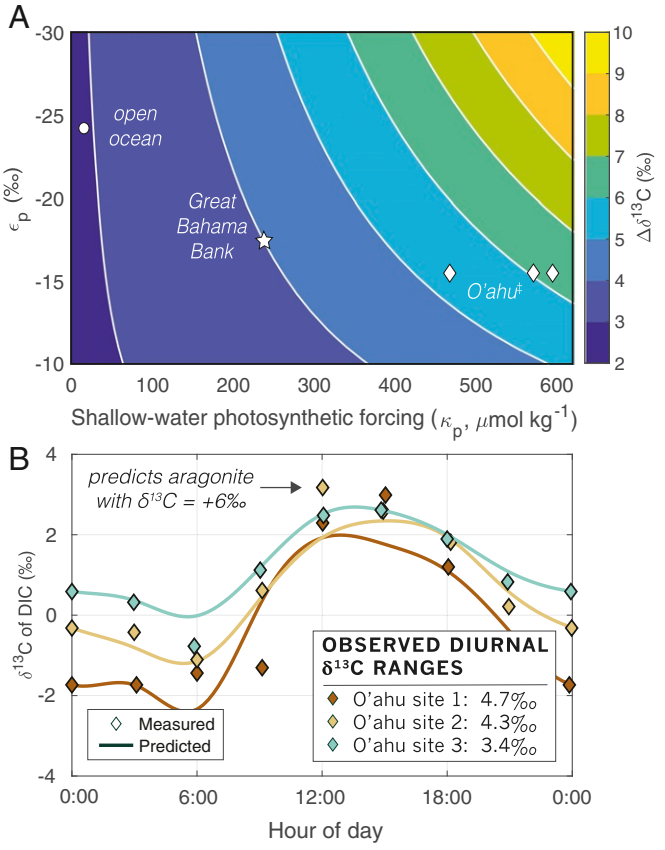

Fig. 6. An exploration of the $\delta^{13}C$ enrichments expected from the diurnal organic carbon mechanism (*A*) and model comparison to observations of diurnal $\delta^{13}C$ variability (*B*). (*A*) The magnitude of carbonate $\delta^{13}C$ enrichment relative to open-ocean DIC ($\Delta\delta^{13}C$) is sensitive to the diurnal photosynthetic transfer of carbon between inorganic and organic reservoirs (κ_p) and the average carbon-isotope fractionation factor between organic matter and local DIC (ϵ_p). The $\delta^{13}C$ enrichment also is sensitive to the saturation state—as Ω_A increases, $\delta^{13}C$ enrichment falls because higher precipitation rates across the entire 24-h cycle cause the nighttime $CaCO_3$ precipitation to constitute a larger proportion of the total $CaCO_3$ flux (*SI Appendix*, Figs. S16 and S17). (*B*) Forced by diurnal TA and DIC measurements from the same water, the engine model accurately predicts changes in the $\delta^{13}C$ of DIC from a shallow coral-reef environment in O'ahu (33). The diurnal cycles in $\delta^{13}C$ of DIC predicted by the engine model also have been observed in other shallow carbonate environments around the world (34) (*SI Appendix*, Fig. S20).

Downloaded by guest on July 13, 2020

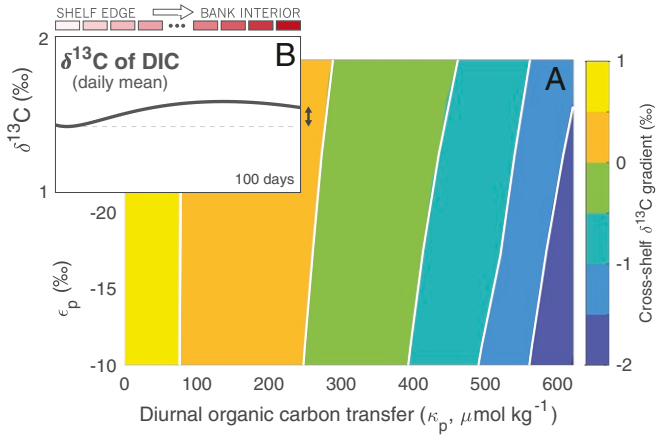

Fig. 7. (*A*) Cross-shelf gradients in sediment $\delta^{13}C$, which we define as the difference between the average $\delta^{13}C$ produced after 100 days of diurnal cycling and the average $\delta^{13}C$ produced after 1 day of diurnal cycling (*B*), as a function of κ_p and ϵ_p. The predicted cross-shelf gradients of $-2‰$ to $+1‰$ are modest relative to the strength of the diurnal carbon engine, which can produce $\delta^{13}C$ enriched by up to $\sim 10‰$ (Fig. 6*A*).

the magnitude of the photosynthetic transfer of carbon between inorganic and organic reservoirs during each diurnal cycle (κ_p), which is a function of both primary productivity and the physical mixing of open marine water with local water, and 2) the $\delta^{13}C$ fractionation factor between DIC and organic matter (ϵ_p), which is a function of growth rate, biology, dissolved CO_2, and surface area/volume (35). Reasonable choices of ϵ_p and κ_p observed in modern reef environments (Fig. 4) induce carbon isotope enrichments of +4 to +7‰ (Fig. 6*A*).

Table 1. Stoichiometry of carbonate precipitation, photosynthesis (16), and air–sea CO_2 gas exchange

Reaction	Equation	*m*
Precipitation	$Ca^{2+} + 2\,HCO_3^- \rightarrow CaCO_3 + CO_2(aq) + H_2O$	−2: −1
Photosynthesis	$106\,CO_2 + 16\,HNO_3 + H_3PO_4 + 122\,H_2O \rightarrow (CH_2O)106\,(NH_3)16\,(H_3PO_4) + 138\,O_2$	16:−106
Gas exchange	$CO_2(aq) \rightarrow CO_2(atm)$	0: 1

m denotes the ΔTA:ΔDIC of the reaction, and corresponds to the slope in Fig. 3*C*.

It may seem counterintuitive that continued production of high $\delta^{13}C$ carbonate does not drive ambient waters toward lower $\delta^{13}C$. However, the precipitation of $CaCO_3$ with $\epsilon_{arag} = +2.7‰$ (1) is inextricably tied to the degassing of CO_2 with $\epsilon_{sea-air} \sim -9.7‰$ (40). Our engine model, undergoing gas exchange as a function of seawater pCO_2 (17) and precipitating carbonate as a function of Ω (31, 32, 41), predicts that carbonate precipitation accounts for 62% of the reduction in banktop DIC, and CO_2 gas escape accounts for the remaining ∼37% (Fig. 5*B*). This estimate is identical to the values inferred from water chemistry measurements (7) (Fig. 2*C*). The net isotopic effect of the coupled carbonate precipitation and gas escape on the $\delta^{13}C$ of DIC is close to zero. Reasonable choices for κ_p or ϵ_p can establish cross-shelf $\delta^{13}C$ gradients in DIC of up to a few per mil (Fig. 7*B*), but the dominant origin of both intra- and intershelf

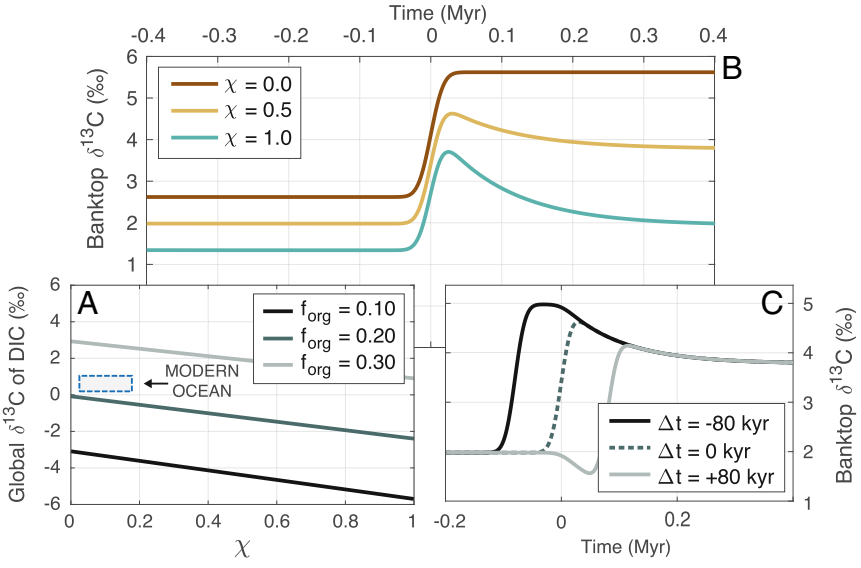

CANNONICAL $\delta^{13}C$ GLOBAL MASS BALANCE EQUATION:

$$\delta^{13}C_{in} = \delta^{13}C_{org} f_{org} + \delta^{13}C_{carb}(1 - f_{org})$$

MODIFIED EQUATION TO DISTINGUISH BETWEEN CARBONATE PRODUCTION ON SHALLOW SHELVES VS. DEEP WATERS:

$$\delta^{13}C_{in} = \delta^{13}C_{org} f_{org} + \chi\delta^{13}C_{shallow}(1 - f_{org}) + (1 - \chi)\delta^{13}C_{deep}(1 - f_{org})$$

Fig. 8. Implications of the diurnal organic carbon engine on global mass balance and the $\delta^{13}C$ records of individual carbonate shelves. (*A*) Relationship between χ, the fraction of global carbonate burial on shallow shelves with active diurnal carbon engines, and the $\delta^{13}C$ of global DIC. Increased χ depresses global DIC to maintain global mass balance. To solve for the curves in (*A*), we adopt a framework similar to that in ref. 36 and use a modified version of the canonical $\delta^{13}C$ mass balance equation (3, 37). In our case, we divide the carbonate burial flux into a shallow flux, where the $\delta^{13}C$ fractionation is +4‰, the empirical enrichment observed in Fig. 1*A*, and a deep flux, where the $\delta^{13}C$ fractionation is +1.1‰, which corresponds to equilibrium calcite in the absence of an active diurnal organic carbon engine (1). Modern global values of $f_{org} \approx 0.20$ to 0.23 (37), $\epsilon_p \approx -23‰$ to $-29‰$ (3, 37), and $\delta^{13}C_{DIC} \approx 0.4‰$ (38, 39) suggest that χ is between 0 and 0.2 today. (*B*) To illustrate the global feedback implied by *A*, we simulate a 3‰ enrichment in $\delta^{13}C$ of precipitated carbonate on shallow shelves around the world. Here, we assume $f_{org} = 0.2$, that the total mass of carbon in the ocean–atmosphere system is in steady-state ($F_{in} = F_{out}$), that the residence time of carbon is 10^5 y (i.e., the modern value) (3), and that the eustatic, evolutionary, or other change prompting the $\delta^{13}C$ enrichment on shallow shelves occurs over a 20-kyr duration. If global shelf area is very low ($\chi \approx 0$), the whole 3‰ enrichment is expressed in shallow carbonates. However, if most global carbonate burial is occurring on shallow shelves ($\chi \approx 1$), the $\delta^{13}C$ enrichment signal is damped to <1‰. The $\delta^{13}C$ spike is not damped all of the way to zero because there remains a second sink of carbon (the burial of organic matter). Thus, the 3‰ enrichment on shallow shelves, which increases the $\delta^{13}C$ offset between carbonate and organic matter, leads to a $0.2 \times 3‰ = 0.6‰$ change in global DIC. (*C*) A change in κ_p and ϵ_p may not start at the same moment everywhere, even if the change eventually is global in nature. Individual shelves experiencing changes in $\delta^{13}C$ enrichment before or after the globally induced depression in $\delta^{13}C$ of DIC would produce $\delta^{13}C$ records that either spike first, before the global negative feedback depresses $\delta^{13}C$, or plunge first from the global signal, before rising due to local $\delta^{13}C$ enrichment.

Downloaded by guest on July 13, 2020

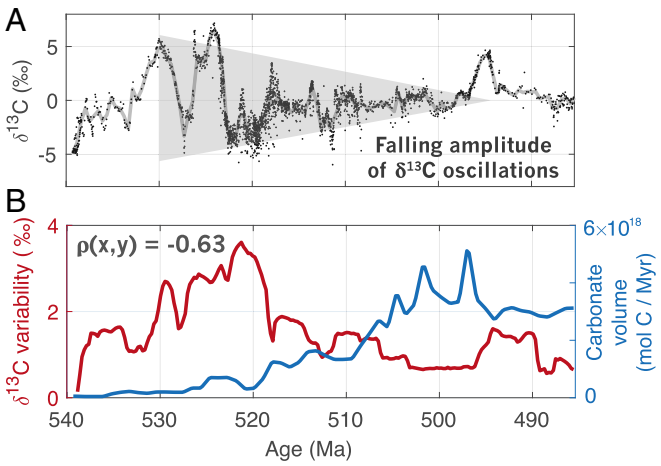

Fig. 9. (*A*) δ^{13}C record through the Cambrian, based on the compilations of refs. 39 and 43. (*B*) The δ^{13}C variability, computed as the SD (1σ) of all δ^{13}C values in a moving window of size $\tau = 3.5$ Ma (43), is strongly anticorrelated with the volume of carbonates preserved in the geologic record of North America (44). Although δ^{13}C variability is a function of the chosen window size, a wide range of window sizes from $\tau = 0 - 10$ Myr yield strong Pearson coefficients $\left(\rho(x,y) = \frac{\mathrm{cov}(x,y)}{\sigma_x \sigma_y}\right)$ with magnitudes greater than 0.6 (*SI Appendix*, Fig. S13).

variability in carbonate δ^{13}C values might result from spatiotemporal variability in κ_p and/or ϵ_p. For example, the full range of κ_p values depicted in Fig. 4*H* is observed in different environments from a single coral reef (42) (*SI Appendix*, Fig. S15), and ϵ_p may vary from -5‰ to -25‰ depending on the relative abundance of photoautotrophs such as cyanobacteria, algae, and seagrass (5).

Implications for the Global Carbon Cycle and the Interpretation of the δ^{13}C Record

The δ^{13}C of shallow carbonates is a crucially important tool for global chemostratigraphic correlation, especially before the appearance of index animal fossils (39, 43, 45). If κ_p and ϵ_p vary within or between shelves, their control on primary δ^{13}C would compound δ^{13}C gradients driven by diagenesis (46) or the influx of terrestrial organic matter (47, 48), adding to the challenges of chemostratigraphic correlation. In contrast, if κ_p and ϵ_p are controlled by evolutionary, eustatic, and/or climate changes, carbonate shelves might respond synchronously with similar shifts in δ^{13}C (49). As the area of shallow shelves increases, the burial of high δ^{13}C carbonates will lower the δ^{13}C of seawater DIC to satisfy global isotope mass balance (Fig. 8*A*). This negative feedback means that, if a global forcing increases the strength of the diurnal carbon engine on all shelves, the magnitude of the positive δ^{13}C shift in shallow carbonate will be damped as a function of global carbonate shelf area (Fig. 8*B*). The "falling amplitude of carbon isotopic oscillations" through the Cambrian (Fig. 9*A*), observed by ref. 50, might be one geologic example of this negative shelf-area feedback; as the volume of preserved carbonates in the geologic record of North America—an imperfect approximation of global shallow carbonate area—increases during the Cambrian (44), the magnitude of δ^{13}C oscillations falls (Fig. 9*B*). Ascribing the 1- to 3-Myr positive excursions in Fig. 9*A* to diurnal carbon-engine phenomena could alleviate the need to call upon unrealistic changes in global carbon cycling (51), and instead may hint at previously unrecognized global forcings to κ_p and/or ϵ_p.

Certainly not all δ^{13}C excursions in the geologic record of shallow carbonates were driven by synchronous changes in κ_p or ϵ_p. However, the diurnal organic carbon engine (Fig. 3*A*) can successfully 1) modulate global DIC, forced by tectonic or eustatic controls on shelf area or biologically induced changes in vital effects, ϵ_p, and κ_p; and 2) explain how a global forcing may be variably expressed with different peak δ^{13}C values (48, 52).

Conclusions

Much of our understanding of ancient Earth history comes from shallow carbonates, as open marine records tend to be subducted at plate margins. However, it is time to recognize that the δ^{13}C record of ancient shallow carbonates may not always directly reflect global carbon cycling. Recent work on marine (46), meteoric (53), and burial (54) diagenesis has illuminated the role of postdepositional alteration. Here, we present a mechanism to explain how the primary δ^{13}C values of the shallow carbonate sink can be partially decoupled from global DIC. Specifically, we have shown how ordinary diurnal carbon cycling is sufficient to produce the most anomalously positive δ^{13}C on shelves today—and perhaps in the geological record—without any net production of oxygen. Although the diurnal carbon engine and subsequent diagenesis complicates interpretations of carbon-isotope chemostratigraphy, frequent comparison of modern analogue studies to ancient records will help resolve shallow carbonate δ^{13}C into a more refined chronicle of paleoenvironment and Earth history.

Materials and Methods

Carbonate surface sediments from North Andros, San Salvador, and Shark Bay (*SI Appendix*, Fig. S1) were rinsed 3 times in deionized water, dried, homogenized using mortar and pestle, and then placed in individual borosilicate glass reaction vessels. The samples were heated to 110°C to remove volatiles, capped and flushed with helium to remove atmospheric gas from the reaction vessels, and finally reacted at 72°C in a GasBench II preparation device coupled to a Sercon continuous-flow isotope-ratio mass spectrometer. The precision and accuracy of δ^{13}C measurements are monitored through analysis of 15 standards for every 57 measured samples. δ^{13}C data are reported in the standard delta notation relative to Vienna Pee Dee Belemnite. Average precision is <0.1‰ (1σ). All sediment δ^{13}C measurements from North Andros, San Salvador, and Shark Bay (Fig. 1*A*) are provided in a spreadsheet (Dataset S1).

ACKNOWLEDGMENTS. Thank you to J. Birch at Small Hope Bay Lodge for making work possible on Andros Island. Also, thank you to A. Cartwright, R. Coakley, N. Hinsey, A. Mackey, A. Marshall, S. Martin, B. Neymor, G. Thompson, L. Whyms, local customs and immigration, and the Bahamas Environment, Science & Technology Commission. C. Allen at Air Flight Charters and D. Reading at Princeton provided logistical support. We thank L. O'Connor and T. Humes for field assistance in the Bahamas. We thank B. Dyer and B. D'Andrea for assistance in San Salvador and D. Holley and the Fenny family in Shark Bay. A. Gagnon inspired us to adapt models for carbonate system dynamics within individual corals to the scale of an entire carbonate bank. Conversations with B. Dyer, M. Bender, W. Broecker, D. Sigman, W. Fischer, J. Grotzinger, J. Husson, J. Dunne, J. Higgins, A.-S. Crüger Ahm, and J. Strauss improved the manuscript. We thank P. Swart and A. Oehlert for generously sharing their data and for thought-provoking discussions. Feedback from Don Canfield, Brad Rosenheim, and 2 anonymous reviewers significantly improved the manuscript. This material is based on work supported by NSF Division of Earth Sciences Grant 1410317 and by the Princeton Environmental Institute at Princeton University through the Smith-Newton Scholars Program. This work also was supported by the Geological Society of America Stephen G. Pollock Student Research Grant, the Evolving Earth Foundation, the High Meadows Foundation, the Sigma Xi Research Society, and the Princeton Geosciences Student Research Fund.

1. M. Rubinson, R. Clayton, Carbon-13 fractionation between aragonite and calcite. *Geochem. Cosmochim. Acta* **33**, 997–1002 (1969).
2. C. Romanek, E. Grossman, J. Morse, Carbon isotopic fractionation in synthetic aragonite and calcite: Effects of temperature and precipitation rate. *Geochem. Cosmochim. Acta* **56**, 419–430 (1992).
3. L. R. Kump, M. A. Arthur, Interpreting carbon-isotope excursions: Carbonates and organic matter. *Chem. Geol.* **161**, 181–198 (1999).
4. P. K. Swart, J. J. G. Reijmer, R. Otto, A re-evaluation of facies on Great Bahama Bank II: Variations in the δ^{13}C, δ^{18}O and mineralogy of surface sediments. *Int. Assoc. Sedimentol. Spec. Publ.* **41**, 47–59 (2009).

Downloaded by guest on July 13, 2020

5. A. M. Oehlert *et al.*, The stable carbon isotopic composition of organic material in platform derived sediments: Implications for reconstructing the global carbon cycle. *Sedimentology* **59**, 319–335 (2012).
6. P. Swart, G. Eberli, The nature of the δ^{13}C of periplatform sediments: Implications for stratigraphy and the global carbon cycle. *Sediment. Geol.* **175**, 115–129 (2005).
7. W. Broecker, T. Takahashi, Calcium carbonate precipitation on the Bahama banks. *J. Geophys. Res.* **71**, 1575–1602 (1966).
8. P. M. M. Harris, S. J. Purkis, J. Ellis, P. K. Swart, J. J. G. Reijmer, Mapping bathymetry and depositional facies on Great Bahama Bank. *Sedimentology* **62**, 566–589 (2015).
9. K. Deffeyes, Carbonate equilibria: A graphic and algebraic approach. *Limnol. Oceanogr.* **10**, 412–426 (1965).
10. E. Lewis, D. Wallace, L. J. Allison, Program developed for CO_2 system calculation (Tech. Rep. ORNL/CDIAC-105, Carbon Dioxide Information Analysis Center, Oak Ridge National Laboratory, 1998).
11. C. D. Keeling *et al.*, Atmospheric carbon dioxide variations at Mauna Loa observatory, Hawaii. *Tellus* **28**, 538–551 (1976).
12. E. C. Shaw, S. R. Phinn, B. Tilbrook, A. Steven, Natural in situ relationships suggest coral reef calcium carbonate production will decline with ocean acidification. *Limnol. Oceanogr.* **60**, 777–788 (2015).
13. E. C. Shaw, B. I. McNeil, B. Tilbrook, Impacts of ocean acidification in naturally variable coral reef flat ecosystems. *J. Geophys. Res. Oceans* **117**, C03038 (2012).
14. R. Albright, J. Benthuysen, N. Cantin, K. Caldeira, K. Anthony, Coral reef metabolism and carbon chemistry dynamics of a coral reef flat. *Geophys. Res. Lett.* **42**, 3980–3988 (2015).
15. A. McMahon, I. R. Santos, T. Cyronak, B. D. Eyre, Hysteresis between coral reef calcification and the seawater aragonite saturation state. *Geophys. Res. Lett.* **40**, 4675–4679 (2013).
16. A. Redfield, On the proportions of organic derivatives in sea water and their relation to the composition of plankton. *James Johnstone Memorial Volume* (University Press of Liverpool, 1934), pp. 176–192.
17. R. Wanninkhof, Relationship between wind speed and gas exchange over the ocean. *J. Geophys. Res. Oceans* **97**, 7373–7382 (1992).
18. R. Wanninkhof, Relationship between wind speed and gas exchange over the ocean revisited. *Limnol Oceanogr. Methods* **12**, 351–362 (2014).
19. D. T. Ho *et al.*, Measurements of air-sea gas exchange at high wind speeds in the Southern Ocean: Implications for global parameterizations. *Geophys. Res. Lett.* **33**, L16611 (2006).
20. P. S. Liss, L. Merlivat, "Air-sea gas exchange rates: Introduction and synthesis" in *The Role of Air-Sea Exchange in Geochemical Cycling*, P. Buat-Ménard, Ed. (D. Reidel Publishing Company, 1986), pp. 113–127.
21. P. D. Nightingale *et al.*, In situ evaluation of air-sea gas exchange parameterizations using novel conservative and volatile tracers. *Glob. Biogeochem. Cycles* **14**, 373–387 (2000).
22. A. Sutton *et al.*, Using present-day observations to detect when anthropogenic change forces surface ocean carbonate chemistry outside preindustrial bounds. *Biogeosciences* **13**, 5065–5083 (2006).
23. F. T. Short, Effects of sediment nutrients on seagrasses: Literature review and mesocosm experiment. *Aquat. Bot.* **27**, 41–57 (1987).
24. J. J. Walsh, Importance of continental margins in the marine biogeochemical cycling of carbon and nitrogen. *Nature* **350**, 53–55 (1991).
25. H. S. Jensen, O. I. Nielsen, M. S. Koch, I. de Vicentea, Phosphorus release with carbonate dissolution coupled to sulfide oxidation in Florida Bay seagrass sediments. *Limnol. Oceanogr.* **54**, 1753–1764 (2009).
26. A. Pannard *et al.*, Production of exopolymers (EPS) by cyanobacteria: Impact on the carbon-to-nutrient ratio of the particulate organic matter. *Aquat. Ecol.* **50**, 29–44 (2016).
27. P. Cook, B. Veuger, S. Böer, J. Middelburg, Effect of nutrient availability on carbon and nitrogen incorporation and flows through benthic algae and bacteria in near-shore sandy sediment. *Aquat. Microb. Ecol.* **49**, 165–180 (2007).
28. M. S. Andres, D. Y. Sumner, R. P. Reid, P. K. Swart, Isotopic fingerprints of microbial respiration in aragonite from Bahamian stromatolites. *Geology* **34**, 973–976 (2006).
29. S. Chen, A. Gagnon, J. Adkins, Carbonic anhydrase, coral calcification and a new model of stable isotope vital effects. *Geochem. Cosmochim. Acta* **236**, 179–197 (2018).
30. E. C. Geyman, A. C. Maloof, A simple method for extracting water depth from multispectral satellite imagery in regions of variable bottom type. *Earth Space Sci.* **6**, 527–537 (2019).
31. E. A. Burton, L. M. Walter, Relative precipitation rates of aragonite and Mg calcite from seawater: Temperature or carbonate ion control? *Geology* **15**, 111–114 (1987).
32. B. N. Opdyke, B. H. Wilkinson, Carbonate mineral saturation state and cratonic limestone accumulation. *Am. J. Sci.* **293**, 217–234 (1993).
33. C. Richardson, H. Dulai, B. Popp, K. Ruttenberg, J. Fackrell, Submarine groundwater discharge drives biogeochemistry in two Hawaiian reefs. *Limnol. Oceanogr.* **62**, 5348–5363 (2017).
34. J. Weber, P. Woodhead, Diurnal variations in the isotopic composition of dissolved inorganic carbon in seawater from coral reef environments. *Geochem. Cosmochim. Acta* **35**, 891–902 (1971).
35. S. Burkhardt, U. Riebsell, I. Zondervan, Effects of growth rate, CO_2 concentration, and cell size on the stable carbon isotope fractionation in marine phytoplankton. *Geochem. Cosmochim. Acta* **63**, 3729–3741 (1999).
36. D. P. Schrag, J. A. Higgins, F. A. Macdonald, D. T. Johnston, Authigenic carbonate and the history of the global carbon cycle. *Science* **339**, 540–543 (2013).
37. J. M. Hayes, H. Strauss, A. J. Kaufman, The abundance of ^{13}C in marine organic matter and isotopic fractionation in the global biogeochemical cycle of carbon during the past 800 Ma. *Chem. Geol.* **161**, 103–125 (1999).
38. P. Kroopnick, The distribution of ^{13}C of ΣCO_2 in the world oceans. *Deep Sea Res. Part A Oceanogr. Res. Pap.* **32**, 57–84 (1985).
39. M. R. Saltzman, E. Thomas, "Carbon isotope stratigraphy" in *Geologic Time Scale 2012*, F. M. Gradstein, J. G. Ogg, M. Schmitz, G. Ogg, Eds. (Elsevier, 2012), pp. 207–232.
40. U. Siegenthaler, K. Munnich, "^{13}C/^{12}C fractionation during CO_2 transfer from air to sea" in *Carbon Cycle Modeling: SCOPE 16*, B. Bolin, Ed. (John Wiley & Sons, 1981), pp. 249–257.
41. C. S. Romanek, J. W. Morse, E. L. Grossman, Aragonite kinetics in dilute solutions. *Aquat. Geochem.* **17**, 339–356 (2011).
42. T. Nakamura, T. Nakamori, Estimation of photosynthesis and calcification rates at a fringing reef by accounting for diurnal variations and the zonation of coral reef communities on reef flat and slope: A case study for the Shiraho reef, Ishigaki Island, southwest Japan. *Coral Reefs* **28**, 229–250 (2009).
43. A. C. Maloof *et al.*, The earliest Cambrian record of animals and ocean geochemical change. *Geol. Soc. Am. Bull.* **122**, 1731–1774 (2010).
44. S. E. Peters, J. M. Husson, J. Czaplewski, Macrostrat: A platform for geological data integration and deep-time earth crust research. *Geochem. Geophys. Geosyst.* **19**, 1393–1409 (2018).
45. G. P. Halverson *et al.*, Toward a Neoproterozoic composite carbon-isotope record. *Geol. Soc. Am. Bull.* **117**, 1181–1207 (2005).
46. J. Higgins *et al.*, Mineralogy, early marine diagenesis, and the chemistry of shallow-water carbonate sediments. *Geochem. Cosmochim. Acta* **220**, 512–534 (2017).
47. W. P. Patterson, L. M. Walter, Depletion of 13C in seawater DIC on modern carbonate platforms: Significance for the carbon isotopic record of carbonates. *Geology* **22**, 885–888 (1994).
48. K. M. Panchuk, C. Holmden, L. R. Kump, Sensitivity of the epeiric sea carbon isotope record to local-scale carbon cycle processes: Tales from the Mohawkian Sea. *Palaeogeogr. Palaeoclimatol. Palaeoecol.* **228**, 320–337 (2005).
49. P. K. Swart, Global synchronous changes in the carbon isotopic composition of carbonate sediments unrelated to changes in the global carbon cycle. *Proc. Natl. Acad. Sci. U.S.A.* **105**, 13741–13745 (2008).
50. M. D. Brasier, S. S. Sukhov, The falling amplitude of carbon isotopic oscillations through the lower to Middle Cambrian: Northern Siberia data. *Can. J. Earth Sci.* **35**, 353–373 (1998).
51. A. C. Maloof *et al.*, Constraints on early Cambrian carbon cycling from the duration of the Nemakit-Daldynian-Tommotian boundary δ^{13}C shift, Morocco. *Geology* **38**, 623–626 (2010).
52. M. E. Patzkowsky, L. M. Slupik, M. A. Arthur, R. D. Pancost, K. H. Freeman, Late middle ordovician environmental change and extinction: Harbinger of the late ordovician or continuation of Cambrian patterns? *Geology* **25**, 911–914 (1997).
53. B. Dyer, J. A. Higgins, A. C. Maloof, A probabilistic analysis of meteorically altered δ^{13}C chemostratigraphy from late Paleozoic ice age carbonate platforms. *Geology* **45**, 135–138 (2017).
54. L. A. Derry, A burial diagenesis origin for the Ediacaran Shuram–Wonoka carbon isotope anomaly. *Earth Planet. Sci. Lett.* **294**, 152–162 (2010).

Downloaded by guest on July 13, 2020